HHS Public Access

Author manuscript

Nucl Med Biol. Author manuscript; available in PMC 2017 May 01.

Published in final edited form as:

Nucl Med Biol. 2016 May ; 43(5): 318–323. doi:10.1016/j.nucmedbio.2016.02.008.

Compartmental Modeling of [^{11}C]MENET Binding to the Norepinephrine Transporter in the Healthy Human Brain

Vikram Adhikarla, **Fanxing Zeng**, **John R. Votaw**, **Mark M. Goodman**, and **Jonathon A. Nye**

Department of Radiology and Imaging Sciences, Emory University, Atlanta, GA 30322

Abstract

Introduction—Dysregulation of the noradrenergic system has been implicated in a number of neurological conditions such as Parkinson's and Alzheimer's. [^{11}C]MENET is a novel PET radiotracer with high affinity and selectivity for the norepinephrine transporter. The applicability of different kinetic models on [^{11}C]MENET PET image quantification in healthy population are evaluated.

Methods—Six healthy volunteers (mean age: 54 years) were recruited for the study, five of whom underwent arterial sampling for measurement of the input function. Ninety minute dynamic PET scans were obtained on a high resolution research tomograph with 15 mCi of [^{11}C]MENET injected at the scan start time. Regions of interest were delineated on the PET scan aided by the corresponding MRI image for anatomical guidance. Distribution volumes and their ratios (DVRs) with respect to the occipital reference tissue were calculated using the full arterial model (FAM), the simplified reference tissue model (SRTM) and the multilinear reference tissue model (MRTM2).

Results—Among the FAMs, the single-tissue model was found to be statistically superior to the two-tissue model. [^{11}C]MENET focal uptake was observed in the NET-rich regions of the brainstem and subcortical regions including the thalamus, locus cereleus and the raphe nuclei. Highest DVRs were observed in the locus cereleus (mean ± standard deviation: 1.39 ± 0.25) and red nucleus (1.35 ± 0.25). DVRs of the thalamus were in good agreement between FAM (1.26 ± 0.13), SRTM (1.23 ± 0.15) and MRTM2 (1.21 ± 0.14). Comparing the FAM to the SRTM and MRTM2, DVRs were underestimated in the thalamus by 3% and 4% on average, respectively.

Conclusion—The single-tissue compartmental model was sufficient in describing the [^{11}C]MENET kinetics in the healthy human brain. SRTM and MRTM2 present themselves as attractive options for estimating NET DVR using an occipital reference region.

Corresponding Author: Jonathon A. Nye, PhD, Wesley Woods Health Center, 1841 Clifton Rd. NE, Atlanta, GA 30329, jnye@emory.edu.

First Author: Vikram Adhikarla, PhD, Wesley Woods Health Center, 1841 Clifton Rd. NE, Atlanta, GA 30329, adhikarla@emory.edu

Financial Disclosure

None of the authors report conflicts of interests with the work presented.

Keywords

norepinephrine; norepinephrine transporter; positron emission tomography; Parkinson's; Alzheimer's; Stress

Introduction

Monoamine neurotransmitters such as norepinephrine (NE), dopamine (DA) and serotonin (5-HT) are critical for our mental wellbeing and have been the targets of extensive research over the past few decades [1, 2]. Among these, norepinephrine is responsible for attention, stress management, as well as working and emotional memory [3, 4]. The reuptake of NE is mediated by the norepinephrine transporter (NET). Dysregulation of NET is implicated in a variety of neurological conditions such as ADHD [5], depression [6], anxiety [7], Parkinson's [8], Alzheimer's [9], epilepsy [10], drug abuse [11] and post-traumatic stress disorder [4]. Thus, reliable quantitation of NET may help monitor patient disease progress and response to therapy. Such quantification is non-invasively possible using positron emission tomography (PET) imaging with a suitable radiotracer.

A number of radiotracers have been developed to estimate the concentration of NET [12, 13]. However, the number of tracers relevant to the human brain has been limited. The primary hurdle remains the non-specific binding of these radioligands *in vivo*. A promising radioligand is ^{11}C labeled (S,S) 2-[(2-methoxyphenoxy)phenylmethyl]morpholine (MeNER), also called methylreboxetine (MRB), having an *in vitro* IC_{50} of 2.5 nM [14]. It has been used to investigate NET density in normal controls, cocaine addicts [11] and obese population [15]. A fluorine analog of MRB, the [^{18}F]FMeNER-D2 has been used to study NET binding density in patients with major depressive disorders [16] and ADHD [17]. [^{18}F]FMeNER-D2 has also been used in an autoradiographic study of the human brain [18]. The locus cereleus, cerebellum, cortex and the thalamus were found to exhibit NET localization. Typically, dissimilar concentrations of NET in thalamus and the locus cereleus and have been used to identify healthy volunteers from patients.

Given the success of reboxetine analogs as NET ligands, Zeng and colleagues developed (2*S*,3*S*)-2-[α-(2-methylphenoxy)phenylmethyl]morpholine (MENET) and radiolabeled it with ^{11}C to synthesize a radioligand with high affinity to NET while being selective against DAT and SERT [19, 20]. [^{11}C]MENET was used *in vitro* and *in vivo* in non-human primates. Compared to [^{11}C]MeNER, [^{11}C]MENET was found to demonstrate more attractive imaging kinetics reaching quasi-equilibrium in less than an hour post-injection in non-human primates. [^{11}C]MeNER uptake in comparison did not reach peak equilibrium during a 90 minute PET measurement and demonstrated a relatively noisy signal during the last quarter of the scan [21].

In the current work, we report the kinetics of [^{11}C]MENET in six healthy human volunteers and evaluate if the density of NET can be measured reliably in different regions of the brain using [^{11}C]MENET. The simplified reference tissue model (SRTM) and the multilinear reference tissue models are compared against the compartmental model with arterial input to investigate simpler quantification methods.

Materials and Methods

Volunteer details

Six male volunteers ranging in age from 43 and 66 years (mean age: 54 ± 8 years) participated in the study after providing written informed consent. All volunteers were considered physically and mentally healthy as judged by the absence of any history of neurological or psychiatric disorders and absence of any active medical conditions. All volunteers underwent a physical examination, baseline electrocardiogram and MINI structured diagnostic interview. Laboratory testing of urine and blood were performed 1 day prior to imaging. None of the volunteers were taking medications that acted on the central nervous system. Finally, volunteers were instructed to fast at least 4 hours prior to the PET study. This study was approved by the Emory University Institutional Review Board and was conducted under the auspices of the FDA as part of an investigational new drug (IND #112806).

Magnetic Resonance Imaging

Structural MRI data was collected on all volunteers to aid in delineation of regions of interest (ROI) on PET images. A 3D T1-weighted MPRAGE of the brain was acquired with a Siemens Magnetom Trio 3-T (Siemens Medical Solutions USA, Malvern, PA). The scan parameters were 1 mm thick images with a transverse plane isotropic pixel size of 0.5 mm (repetition time/echo time 2500/4.38 msec, inversion time 900 ms, flip angle 10^0, acquisition field-of-view 320 × 192 pixels, matrix size 320 × 320 pixels).

PET Imaging Procedure

All volunteers were scanned on a Siemens High Resolution Research Tomograph (HRRT) (Seimens Medical Solutions, Knoxville, TN) in the supine position. The HRRT has a 24/31 cm axial/transaxial field of view (FOV) and reconstructed image resolution of 2.4 mm in all directions. The volunteer's head was restrained using straps placed over the forehead and real-time motion monitoring was performed with a Polaris Vicra infrared stereo camera (NDI Medical, Waterloo, Ontario, Canada). Arterial blood samples were acquired for five (volunteer 1 – 5) of the six volunteers. A catheter was placed in the radial vein for administration of [^{11}C]MENET. A second catheter was placed in the radial artery on the opposite arm under local anesthesia for arterial blood sampling. [^{11}C]-MENET was obtained by methylation of (2*S*,3*S*)-*N*-*tert*-Butoxycarbonyl-2-[r-(2-trimethylstannylphenoxy)phenylmethyl]morpholine with ^{11}C-CH_3I as previously described [20]. A 90 min emission list mode scan was started simultaneously with a 5 min constant bolus infusion of [^{11}C]MENET using a syringe pump. Emission list mode data were binned into the following framing sequence: 6 × 30 s, 4 × 180 s, 5 × 300 s, 5 × 600 s. Attenuation correction was measured post-emission by acquiring transmission data with a Cs-137 point source [22]. Data were reconstructed with an ordinary-poisson ordered subset expectation maximization (OP-OSEM) using 6 iterations and 16 subsets. Image data were post-filtered with 4mm Gaussian kernel giving an in-place resolution of 4.7 mm.

Arterial samples were collected by hand in 1.5 mL aliquots every 10 seconds for the first two minutes. This was followed by every 30 seconds up to five minutes, every 60 seconds up

to ten minutes, and then at 15, 20, 30 and 60 minutes. Samples were chilled and centrifuged to separate the plasma fraction from the red blood cells and proteins. 100 uL aliquots of the plasma rich supernatant were counted in duplicate on a NaI Packard Cobra well-counter (Perkin-Elmer, Waltham, MA.) and decay corrected to the injection time. Six additional larger samples (5 mL) were collected at 4.5, 6, 10, 20, 30, 60 minutes post [^{11}C]MENET injection in EDTA to determine the ratio of parent compound to its metabolic derivatives. These samples were deproteinized by the addition of 0.7 mL acetonitrile, vortexed for one minute and centrifuged as described above to recover the protein-free plasma supernatant. The protein free plasma was then filtered and injected onto a reverse phase Waters Xterra RP 18 HPLC column coupled to a radiometric detector to determine the percent parent. Parent blood activity concentrations for each subject were converted to standardized uptake values (SUV) and fitted to a piecewise sum of two Gaussians with three exponentials to serve as the individual arterial input to the compartment model.

Data Analysis

Head motion was corrected in volunteers exhibiting greater than 4 mm head motion using a multiple-acquisition-frame approach described by Herzog and colleagues [23]. Briefly, the attenuation map was aligned to the non-attenuation corrected emission reconstruction using rigid-body transformations and optimization of the mutual information metric. Emission data was then reconstructed with attenuation and scatter correction performed using the aligned transmission maps. Intra-frame alignment was performed on the final reconstructed data with the same optimization metric.

Arterial input compartment model—Two compartmental models were implemented: a single-tissue model (1TC) with two rate constants (K_1 and k_2) and a two-tissue model (2TC) with four rate constants (K_1, k_2, k_3, and k_4). K_1 [mL/g/min] and k_2 [1/min] represent the unidirectional fractional rate constants, corresponding to the influx and efflux of radioligand diffusion across the blood brain barrier, respectively. k_3 [1/min] and k_4 [1/min] represent the radioligand association and dissociation rate to the specific binding sites, respectively. The blood volume was fixed to 3%. The above parameters were determined for each region by an iterative nonlinear least squares fit using the Powell method implemented in IDL (Interactive Data Language, ITT Visual Solutions Inc., Boulder, CO) as previously described [24].

The dynamic PET imaging data was summed over all frames and the resultant image for each volunteer was co-registered with their corresponding MRI for localization of regions of interest (ROI). The regions implicated for NET by Schou *et al* [18] along with other regions of the brain exhibiting relatively high uptake were delineated. Neuroanatomical atlas by Haines [25] and regions of focal uptake on the PET image were used to guide ROI delineation. The complete list of segmented ROIs includes caudate, cerebellum, frontal cortex, locus cereleus, midbrain raphe (nucleus raphe dorsalis), occipital lobe, putamen, red nucleus and the thalamus. Bilateral regions were pooled, and ROIs transferred to each PET frame were then corrected for radioactive decay to generate the time-activity curves with the activity converted to SUV. A representation of these regions can be visualized in the sagittal cross-section through the average SUV PET (30 – 90 minutes) and MRI images of volunteer 2 (figure 1).

The distribution volumes characterizing the receptor densities in different ROIs were obtained using the following three techniques:

a. Compartmental modeling using arterial input.

b. Three parameter simplified reference tissue model (SRTM) with a single-tissue compartment for both reference tissue and tissue of interest.

c. The multilinear reference tissue model (MRTM2) [26].

Details regarding the calculation of the distribution volumes can be found in literature [27, 28]. The distribution volume ratios between the ROI and the reference tissue are calculated using each of the techniques. Distribution volume ratios (DVRs) were calculated using the occipital lobe as the reference region. The occipital lobe has been found to have one of the lowest concentrations of NET [19, 29] and has thus been used as a reference region in earlier works [11, 15].

Data presentation

Temporal changes in both the measured activity and the metabolite percentage are shown. Time activity curves for four regions with significantly different peak times are analyzed: occipital lobe, thalamus, red nucleus and the locus cereleus.

The suitability of the single-tissue compartmental model (1TC) and the two-tissue compartmental model (2TC) were evaluated against the data to identify which model was more appropriate describing the dynamics of [^{11}C]MENET uptake in the ROIs. The statistical superiority of the models was tested using the Akaike Information Criterion (AIC) in each region and results of the thalamus are reported in the results. Distribution volumes and distribution volume ratios are calculated and tabulated for all three techniques. Lastly, the stability of the thalamus distribution volume ratios for time-activity data training from 60 to 90 minutes were analyzed. Data points were removed sequentially from the time activity curves starting at 90 min and the DVRs were derived using the 1TC model.

Results

Injected and specific activities (mean ± standard deviation) of [^{11}C]MENET at the scan start time were 14.6 ± 0.5 mCi and 0.88 ± 0.12 Ci/μmol respectively. The peak activity for arterial input samples collected from the radial artery peaked within five minutes post-injection (figure 2). The tracer was metabolized rapidly within the first twenty minutes post-injection and the metabolite percentage of the total activity was roughly 50% by the end of an hour.

Radiotracer accumulation in different regions of interest occurred at different rates and thus peaks in radiotracer activity were obtained at different times. Representative (volunteer 4) time-activity curves for occipital lobe, thalamus, red nucleus and the locus cereleus are shown in figure 3. Peak radiotracer activity was achieved earliest (25 – 30 minutes post-injection) in the occipital lobe and latest in the locus cereleus (post 60 minutes). The order in which the ROIs exhibited peak radioactivity is as follows: occipital lobe < thalamus < red nucleus < locus cereleus. Data for the red nucleus and the locus cereleus was noisier compared to the other two regions reflecting the uncertainties that plague the activity

measurement in smaller ROIs. Additionally, the thalamus registered the highest activity among the segmented ROIs at peak uptake.

In all the analyzed regions for volunteers 1 through 5, both the 1TC and the 2TC compartmental models converged to yield solutions identifying the involved model constants (table 1). However, the parameter ratios k_3/k_4 and $(K_1/k_2)\times(1+k_3/k_4)$ for the 2TC model were not stable. The distribution volumes of the thalamus calculated using both the 1TC and the 2TC compartmental models were similar and ranged from 2.37 – 2.80 mL/g except for volunteer 3 where the distribution volume was lower; likely due to the impact of motion (maximum displacement: 4 cm). The mean ± standard deviations of the thalamus distribution volumes with and without including the motion corrected volunteer were 2.42 ± 0.40 mL/g and 2.59 ± 0.17 mL/g respectively. In all the fits, the 1TC model and the 2TC model fits were nearly identical as seen from the identical residual sum of squares (RSS) between the model fit and the data points. In all the volunteers the 1TC model was found to be statistically superior compared to the 2TC model as determined by the Akaike Information Criterion.

The average distribution volumes (V_T) using the compartmental model with arterial input ranged from 1.83 – 2.67 mL/g (table 2). Among the regions analyzed, the locus cereleus demonstrated the highest distribution volume, albeit with high uncertainty. The cerebellum on the other hand demonstrated the lowest distribution volume which was comparable to the distribution volumes observed in the caudate and the occipital lobe where the concentrations of NETs are generally low.

Comparison of the distribution volume ratios (DVRs) calculated using all three techniques is shown in table 3. Average DVRs for different regions ranged between 0.95 and 1.39. Reference tissue based DVRs were lower than those calculated using the 1TC model. A comparison of techniques shows that the locus cereleus is one of the regions demonstrating highest DVRs along with the highest uncertainties. Similar DVRs and uncertainties were found in the red nucleus. Lowest DVRs were observed for the cerebellum. Thalamus DVRs were comparable between the three techniques. The uncertainty associated with the thalamus DVR is also lower compared to other regions of interest. Average DVRs (for volunteers 1 through 5) calculated using 1TC, SRTM and MRTM2 were 1.26 ± 0.13, 1.23 ± 0.15 and 1.21 ± 0.14 respectively. On average, SRTM and MRTM2 underestimated the thalamus DVR by 3% and 4% respectively compared to the 1TC model. These underestimations for all ROIs combined were 4% and 6% respectively.

Analysis of the thalamus distribution volume ratios using 1TC model shows that the distribution volumes were temporally stable with low uncertainties. Thalamus DVR at 55 minutes post-injection was 1.33 ± 0.04 and decreased to 1.26 ± 0.13 at 85 minutes. The higher uncertainty 85 minutes post-injection is attributed to motion artifacts in volunteer 3 dataset. If this particular dataset is ignored, then the distribution volume ratio 85 minutes post-injection remains stable at 1.32 ± 0.05.

Discussion

The single-tissue (1TC) model was found to be sufficient for describing the tracer kinetics of [^{11}C]MENET in the healthy human brain. While longer imaging durations might shed more light on the appropriateness of the 2TC model, the fits within the imaged scan duration between the two models were very similar. For smaller regions like the locus cereleus, the 1TC and the 2TC fits were found to be qualitatively different in some cases, but comparison of the fits with the measured TAC data resulted in similar RSS values.

Locus cereleus and the red nucleus presented the highest V_Ts, but also exhibited high uncertainty; a characteristic inherent of smaller regions of interest. Other reasons for increased uncertainty in small ROIs can be attributed to either motion or the partial volume effects (PVE). Larger regions like the thalamus are not substantially affected by these uncertainties and thus the thalamus presented low V_T variation within the ROIs of higher V_Ts. While the hypothalamus has been found to be a region of high uptake while using [^{11}C](S,S)MRB [30], it was also not found in the current case while using [^{11}C]MENET. A similar result was found in an autoradiography study performed by Schou et al [18]. The lower density of NETs in the hypothalamus was implicated as a possible reason.

Two other studies that have evaluated NET distribution using molecular imaging are ones by Logan *et al* using [^{11}C](S,S)MRB [30] and Arakawa *et al* using [^{18}F](S,S)FMeNER-D_2 [31]. Thalamus binding potentials calculated with respect to the occipital lobe were well matched between the above two radiotracers and [^{11}C]MENET. Thalamus binding potentials (BP_{ND}) calculated using [^{11}C](S,S)MRB [30] and [^{18}F](S,S)FMeNER-D_2 [31] are 0.45 and 0.54 respectively. Average thalamus BP_{ND} (calculated as DVR-1) observed using [^{11}C]MENET is 0.26 which is lower than the above works. However, the mean age of the volunteers in the studies by Logan *et al* and Arakawa *et al* was roughly 30 [30] and 23 [31] years respectively, which is markedly younger from the mean age of the volunteers in the current study (54 years). Age related loss of NET density and the corresponding reduction in DVRs [11] is a significant factor that impacts the comparison of [^{11}C](S,S)MRB and [^{18}F](S,S)FMeNER-D_2 with [^{11}C]MENET.

Measurement of the arterial input function is an arduous and painful process for the patient. Reference tissue techniques can be useful in avoiding the measurement of the arterial input. Comparison of the distribution volume ratios (DVRs) using a reference tissue (table 3) shows that both SRTM and MRTM2 yield lower DVRs than when using the arterial input. The bias in the reference tissue methods can potentially be attributed to specific binding within the reference region as well as non-uniform non-specific binding among different regions [32]. Logan and colleagues showed that occipital lobe was an imperfect reference tissue but suitable for distinguishing differences between controls and treatment groups [29]. In their autoradiography study, Schou *et al* [18] observed (S,S)-[^{18}F]FMeNER-D_2 specific binding in the occipital cortex to be lowest and comparable to the caudate and the putamen. Consequently, the caudate has also been used as a potential reference region [30, 31]. In the current study, thalamus distribution volume ratios analyzed using the caudate as the reference region were slightly lower (1.22 ± 0.09) than the ones calculated using the occipital reference tissue (1.26 ± 0.13) and the cerebellum reference tissue (1.33 ± 0.15).

[^{11}C]MENET distribution volumes for all three regions were comparable with the cerebellum demonstrating the lowest DVRs on average (table 2). These low DVRs of the cerebellum are consistent for the 1TC model as well as the SRTM and the MRTM2. This indicates that both cerebellum and the occipital lobe could serve as reference regions for future analysis.

Thalamus distribution volume ratios between the 1TC model and the reference tissue techniques were comparable making it a viable option for comparison studies. MRTM2 being straightforward to implement, is a useful technique to estimate DVRs. However, MRTM2 requires k_2' (reference region k_2) to be fixed from MRTM1 regression fit. Low NET density regions and regions of small volume are susceptible to noise and motion; making the estimation of k_2' troublesome. In some cases MRTM1 k_2' calculated for these regions was negative and MRTM1 k_2' calculated for the thalamus of that volunteer was used in its stead. Thalamus being a region of substantial volume and significant radiotracer uptake was deemed appropriate to determine the k_2' for that volunteer.

Patients with neurological disorders often find it challenging to remain motionless during the entire duration of the PET scan. While this is of lesser importance for larger regions like the thalamus and occipital lobe, quantification of kinetic parameters for small regions such as the locus cereleus are likely to be impacted. This was the case with volunteer 3, where distribution volume within the thalamus (and other regions) was lower than other that of other volunteers. The time activity curves for the smaller ROIs were also noisy during the later time points of the scan. Motion-correction algorithms need to be employed in such cases to maintain the needed resolution for quantification of small structures such as the locus cereleus. Although motion correction strategies were applied to volunteer 3's data, intra- and inter-frame motion could still not be completely eliminated. Thus, shorter scan durations can facilitate more reliable quantification of the distribution volume ratios in situations of patient motion that occurs later in the scan duration. Thalamus DVRs evaluated using [^{11}C]MENET in the current study were found to be stable between the 60 and 90 minutes post radiotracer injection, supporting the use of scan durations of 60 minutes when evaluating thalamus DVRs. DVR evaluation in smaller sub-cortical nuclei such as the locus cereleus might however benefit from longer scan durations due to their slower kinetics. This observation is in agreement with the study by Ding *et al* [11] where a scan duration of 120 minutes was used to improve accuracy of the DVRs in the locus cereleus and raphe nuclei.

Conclusions

The kinetic parameters estimated from arterial and reference tissue input models successfully characterize the kinetics of [^{11}C]MENET uptake in different regions of the brain. The single-tissue compartmental model with two parameters was found to be sufficient for analysis of the NET concentration in the brain. While the reference tissue techniques slightly underestimated the distribution volume ratios, there was good agreement in the distribution volume ratios between the single-tissue model, the simplified reference tissue model and the multilinear reference tissue model for the thalamus. Thus, monitoring NET concentration within the thalamus using [^{11}C]MENET is an attractive proposition for evaluation of changes in patient condition.

Acknowledgments

This work was supported in part by PHS Grant UL1 RR025008 from the Clinical and Translational Science Award Program, National Institutes of Health, National Center for Research Resource. [^{11}C]MENET was prepared by the Emory Center for Systems Imaging Radiopharmacy Team of Ronald Crowe (BCNP), Michael Shane Waldrep and Karen Dolph (NP).

References

1. Hamon M, Blier P. Monoamine neurocircuitry in depression and strategies for new treatments. Prog Neuropsychopharmacol Biol Psychiatry. 2013; 45:54–63. [PubMed: 23602950]
2. Iversen L. Neurotransmitter transporters: fruitful targets for CNS drug discovery. Mol Psychiatry. 2000; 5(4):357–62. [PubMed: 10889545]
3. van Stegeren AH. The role of the noradrenergic system in emotional memory. Acta Psychol (Amst). 2008; 127(3):532–41. [PubMed: 18070612]
4. O'Donnell T, Hegadoren KM, Coupland NC. Noradrenergic mechanisms in the pathophysiology of post-traumatic stress disorder. Neuropsychobiology. 2004; 50(4):273–83. [PubMed: 15539856]
5. Bobb AJ, et al. Support for association between ADHD and two candidate genes: NET1 and DRD1. Am J Med Genet B Neuropsychiatr Genet. 2005; 134B(1):67–72. [PubMed: 15717291]
6. Moret C, Briley M. The importance of norepinephrine in depression. Neuropsychiatr Dis Treat. 2011; 7(Suppl 1):9–13. [PubMed: 21750623]
7. Kalk NJ, Nutt DJ, Lingford-Hughes AR. The role of central noradrenergic dysregulation in anxiety disorders: evidence from clinical studies. J Psychopharmacol. 2011; 25(1):3–16. [PubMed: 20530586]
8. Del Tredici K, Braak H. Dysfunction of the locus coeruleus-norepinephrine system and related circuitry in Parkinson's disease-related dementia. J Neurol Neurosurg Psychiatry. 2013; 84(7):774–83. [PubMed: 23064099]
9. Chalermpalanupap T, et al. Targeting norepinephrine in mild cognitive impairment and Alzheimer's disease. Alzheimers Res Ther. 2013; 5(2):21. [PubMed: 23634965]
10. Giorgi FS, et al. The role of norepinephrine in epilepsy: from the bench to the bedside. Neurosci Biobehav Rev. 2004; 28(5):507–24. [PubMed: 15465138]
11. Ding YS, et al. PET imaging of the effects of age and cocaine on the norepinephrine transporter in the human brain using (S,S)-[(11)C]O-methylreboxetine and HRRT. Synapse. 2010; 64(1):30–8. [PubMed: 19728366]
12. Schou M V, Pike W, Halldin C. Development of radioligands for imaging of brain norepinephrine transporters in vivo with positron emission tomography. Curr Top Med Chem. 2007; 7(18):1806–16. [PubMed: 17979789]
13. Stehouwer JS, Goodman MM. Fluorine-18 Radiolabeled PET Tracers for Imaging Monoamine Transporters: Dopamine, Serotonin, and Norepinephrine. PET Clin. 2009; 4(1):101–128. [PubMed: 20216936]
14. Melloni P, et al. Potential antidepressant agents. α-Aryloxy-benzyl derivatives of ethanolamine and morpholine. European journal of medicinal chemistry. 1984; 19(3):235–242.
15. Li CS, et al. Decreased norepinephrine transporter availability in obesity: Positron Emission Tomography imaging with (S,S)-[(11)C]O-methylreboxetine. Neuroimage. 2014; 86:306–10. [PubMed: 24121204]
16. Nogami T, et al. Occupancy of serotonin and norepinephrine transporter by milnacipran in patients with major depressive disorder: a positron emission tomography study with [(11)C]DASB and (S,S)-[(18)F]FMeNER-D(2). Int J Neuropsychopharmacol. 2013; 16(5):937–43. [PubMed: 23067569]
17. Vanicek T, et al. The norepinephrine transporter in attention-deficit/hyperactivity disorder investigated with positron emission tomography. JAMA Psychiatry. 2014; 71(12):1340–9. [PubMed: 25338091]
18. Schou M, et al. Post-mortem human brain autoradiography of the norepinephrine transporter using (S,S)-[18F]FMeNER-D2. Eur Neuropsychopharmacol. 2005; 15(5):517–20. [PubMed: 16139169]

19. Zeng F, et al. Synthesis, radiosynthesis, and biological evaluation of carbon-11 and fluorine-18 labeled reboxetine analogues: potential positron emission tomography radioligands for in vivo imaging of the norepinephrine transporter. J Med Chem. 2009; 52(1):62–73. [PubMed: 19067522]
20. Zeng F, et al. An improved synthesis of [11C]MENET via Suzuki coupling with [11C]methyl iodide. J Labelled Comp Radiopharm. 2013; 56(5):307–9. [PubMed: 24285377]
21. Schou M, et al. Specific in vivo binding to the norepinephrine transporter demonstrated with the PET radioligand, (S,S)-[11C]MeNER. Nucl Med Biol. 2003; 30(7):707–14. [PubMed: 14499328]
22. Keller SH, Svarer C, Sibomana M. Attenuation correction for the HRRT PET-scanner using transmission scatter correction and total variation regularization. IEEE Trans Med Imaging. 2013; 32(9):1611–21. [PubMed: 23661313]
23. Herzog H, et al. Motion artifact reduction on parametric PET images of neuroreceptor binding. J Nucl Med. 2005; 46(6):1059–65. [PubMed: 15937320]
24. Votaw JR, et al. Measurement of dopamine transporter occupancy for multiple injections of cocaine using a single injection of [F-18]FECNT. Synapse. 2002; 44(4):203–10. [PubMed: 11984856]
25. Haines, DE. Neuroanatomy, An Atlas of Structures, Sections, and Systems. 4. Baltimore, Maryland: Williams & Wilkins; 1994.
26. Ichise M, et al. Linearized reference tissue parametric imaging methods: application to [11C]DASB positron emission tomography studies of the serotonin transporter in human brain. J Cereb Blood Flow Metab. 2003; 23(9):1096–112. [PubMed: 12973026]
27. Koeppe RA, et al. Compartmental analysis of [11C]flumazenil kinetics for the estimation of ligand transport rate and receptor distribution using positron emission tomography. J Cereb Blood Flow Metab. 1991; 11(5):735–44. [PubMed: 1651944]
28. Innis RB, et al. Consensus nomenclature for in vivo imaging of reversibly binding radioligands. J Cereb Blood Flow Metab. 2007; 27(9):1533–9. [PubMed: 17519979]
29. Logan J, et al. Modeling and analysis of PET studies with norepinephrine transporter ligands: the search for a reference region. Nucl Med Biol. 2005; 32(5):531–42. [PubMed: 15982584]
30. Logan J, et al. Imaging the norepinephrine transporter in humans with (S,S)-[11C]O-methyl reboxetine and PET: problems and progress. Nucl Med Biol. 2007; 34(6):667–79. [PubMed: 17707807]
31. Arakawa R, et al. Quantitative analysis of norepinephrine transporter in the human brain using PET with (S,S)-18F-FMeNER-D2. J Nucl Med. 2008; 49(8):1270–6. [PubMed: 18632811]
32. Salinas CA, Searle GE, Gunn RN. The simplified reference tissue model: model assumption violations and their impact on binding potential. J Cereb Blood Flow Metab. 2015; 35(2):304–11. [PubMed: 25425078]

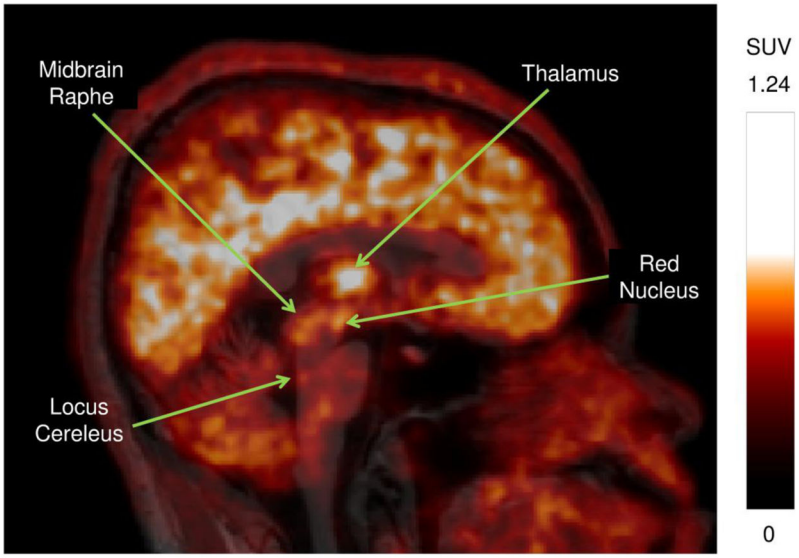

Figure 1.

Sagittal cross-section of the average (30 – 90 minutes) PET SUV image for volunteer 2 overlaid on the corresponding MRI image showing the major regions of interest. 15 mCi of [^{11}C]MENET was injected at the start of the scan that was acquired for 90 minutes.

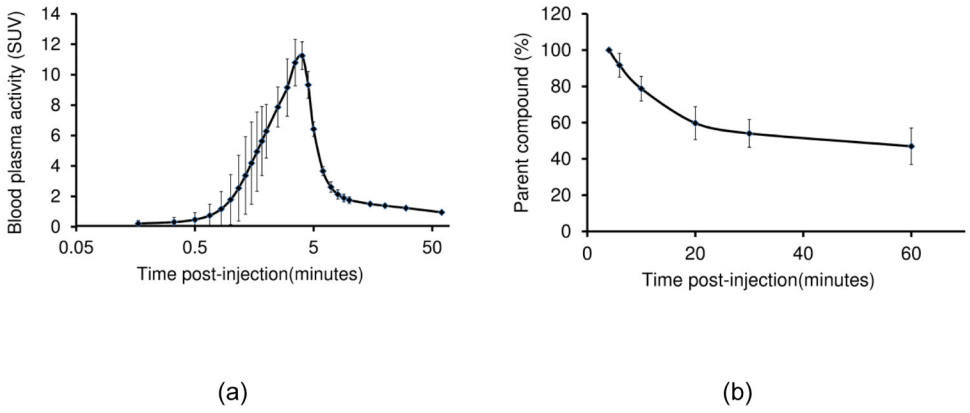

Figure 2.

Tracer kinetics in blood plasma. (a) Parent compound activity concentration measured in the blood plasma. (b) Temporal changes parent compound metabolism. Error bars represent the standard deviation.

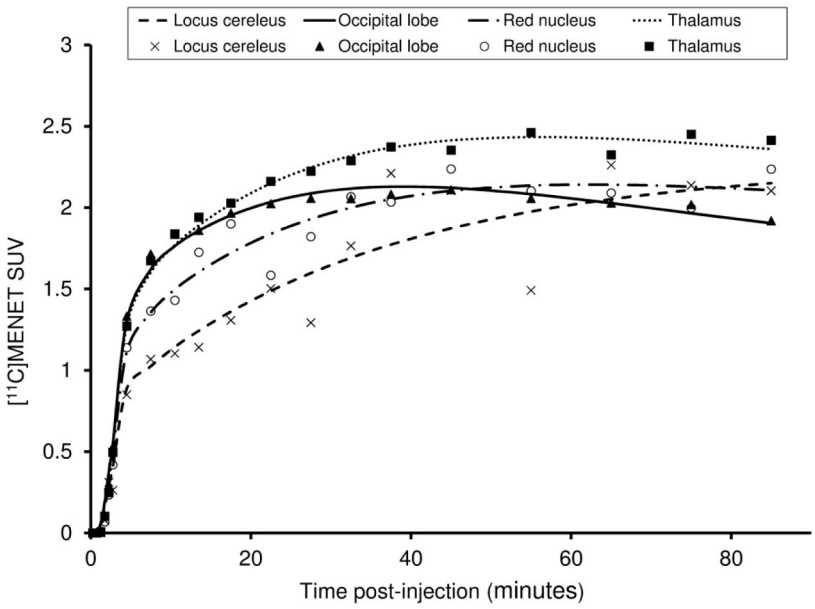

Figure 3.

Time activity curves of different regions of interest (volunteer 4) showing variations in the peak uptake time.

Table 1

Statistical comparison of the single-tissue (1TC) and the two-tissue (2TC) compartmental models with arterial input (for the thalamus).

Volunteer No.	Parameters	K_1 (mL/min/g)	k_2 (1/min)	k_3 (1/min)	k_4 (1/min)	V_T (mL/g)	RSS	AIC
1	2	0.041	0.017			2.37	0.39	−75
	4	0.033	0.020	0.979	2.312	2.37	0.39	−71
2	2	0.043	0.017			2.55	0.06	−113
	4	0.035	0.028	1.200	1.156	2.55	0.06	−109
3	2	0.034	0.019			1.77	0.40	−99
	4	0.027	0.027	1.494	2.028	1.77	0.40	−95
4	2	0.056	0.020			2.80	0.06	−112
	4	0.046	0.039	0.943	0.685	2.80	0.06	−108
5	2	0.044	0.017			2.63	0.29	−80
	4	0.035	0.015	0.269	1.972	2.65	0.29	−76

Table 2

Rate constants and distribution volumes for the single-tissue model (1TC) using arterial input.

Region	Mean ± SD		
	K_1 (mL/min/g)	k_2 (1/min)	V_T (mL/g)
Locus Cereleus	0.027 ± 0.004	0.010 ± 0.002	2.67 ± 0.63
Red Nucleus	0.033 ± 0.009	0.013 ± 0.004	2.55 ± 0.31
Thalamus	0.044 ± 0.008	0.018 ± 0.002	2.42 ± 0.40
Midbrain Raphe	0.034 ± 0.007	0.015 ± 0.004	2.34 ± 0.67
Putamen	0.049 ± 0.009	0.022 ± 0.003	2.28 ± 0.33
Frontal Lobe	0.042 ± 0.007	0.020 ± 0.001	2.08 ± 0.23
Caudate	0.042 ± 0.007	0.021 ± 0.001	1.98 ± 0.32
Occipital lobe	0.048 ± 0.007	0.025 ± 0.002	1.91 ± 0.17
Cerebellum	0.043 ± 0.010	0.023 ± 0.002	1.83 ± 0.28

Table 3

Distribution volume ratios (mean ± standard deviation) calculated using the single-tissue full arterial model, the simplified reference tissue model and the multilinear reference tissue model.

Region	Distribution volume ratios (DVR)		
	1TC (n=5)	SRTM (n=6)	MRTM2 (n=6)
Locus Cereleus	1.39 ± 0.25	1.31 ± 0.17	1.21 ± 0.31
Red Nucleus	1.35 ± 0.25	1.15 ± 0.24	1.12 ± 0.22
Thalamus	1.26 ± 0.13	1.21 ± 0.15	1.19 ± 0.13
Midbrain Raphe	1.22 ± 0.32	1.15 ± 0.24	1.10 ± 0.22
Putamen	1.19 ± 0.09	1.16 ± 0.06	1.14 ± 0.05
Frontal Lobe	1.09 ± 0.05	1.04 ± 0.05	1.04 ± 0.04
Caudate	1.04 ± 0.12	1.01 ± 0.13	1.00 ± 0.13
Cerebellum	0.95 ± 0.08	0.94 ± 0.08	0.94 ± 0.08